Acta Mech 234, 4977–4995 (2023)
https://doi.org/10.1007/s00707-023-03639-7

ORIGINAL PAPER

S. S. Askar · Ahmed E. Abouelregal · A. Foul · Hamid M. Sedighi

Pulsed excitation heating of semiconductor material and its thermomagnetic response on the basis of fourth-order MGT photothermal model

Received: 29 March 2023 / Revised: 27 May 2023 / Accepted: 18 June 2023 / Published online: 10 July 2023
© The Author(s), under exclusive licence to Springer-Verlag GmbH Austria, part of Springer Nature 2023

Abstract When designing mechanical equipment, it's important to consider the photothermal impacts in addition to mechanical ones. This is because photothermal effects can have a significant influence on equipment performance. In this paper, a new theory of thermo-photoelasticity is presented that explains the processes of photoelectron carriers and heat transport in homogeneous and isotropic viscoelastic semiconductor materials. The proposed model combines fourth-order Moore–Gibson–Thompson (MGT) thermoelasticity with the coupled plasma equation. We also include the viscoelastic linear Kelvin–Voigt model, which represents the viscous nature of matter, as part of the model derivation process. We study the problem of a thermoelastic semiconductor medium with stable elastic properties and its traction-free surface exposed to heat flux in the form of laser pulses. To provide analytical solutions for all the variables studied, we use the normal mode approach as the methodology. Furthermore, we estimate the effects of laser pulse rise time, viscosity, and thermal parameters on all fields studied with the help of some comparisons displayed in different illustrations.

List of symbols

λ_e, μ_e	Elastic constants
α_t	Coefficient of thermal expansion
α_1, α_2	Viscoelastic relaxation times
$\gamma = (3\lambda + 2\mu)\alpha_t$	Thermal coupling coefficient
T_0	Initial temperature
$\theta = T - T_0$	Temperature increment

S. S. Askar · A. Foul
Department of Statistics and Operations Research, College of Science, King Saud University, P.O. Box 2455, Riyadh 11451, Saudi Arabia
e-mail: saskar@ksu.edu.sa

A. Foul
e-mail: abdefoul@ksu.edu.sa

A. E. Abouelregal (✉)
Department of Mathematics, College of Science and Arts, Jouf University, Al-Qurayyat 77455, Saudi Arabia
e-mail: ahabogal@gmail.com

A. E. Abouelregal
Department of Mathematics, Faculty of Science, Mansoura University, Mansoura 35516, Egypt

H. M. Sedighi (✉)
Mechanical Engineering Department, Faculty of Engineering, Shahid Chamran University of Ahvaz, Ahvaz, Iran
e-mail: h.msedighi@scu.ac.ir; hmsedighi@gmail.com

H. M. Sedighi
Drilling Center of Excellence and Research Center, Shahid Chamran University of Ahvaz, Ahvaz, Iran

T	Absolute temperature
C_e	Specific heat
$e = \text{div } \mathbf{u}$	Cubical dilatation
σ_{ij}	Stress tensor
e_{ij}	Strain tensor
N	Carrier density
$\overrightarrow{H}$	Heat flow vector
$\boldsymbol{u}$	Displacement vector
$\overrightarrow{X}$	Position vector
$\overrightarrow{F}$	External force vector
μ_0	Magnetic permeability
K	Thermal conductivity
ρ	Material density
Q	Heat source
K^*	Ate of thermal conductivity
δ_{ij}	Kronecker′s delta function
∇^2	Laplacian operator
τ_q	Phase lag of heat flow
τ_θ	Phase lag of temperature gradient
d_n	Electronic deformation coefficient
E_{g}	Semiconductor gap energy
κ	Thermal activation coupling parameter
$\gamma_n = (3\lambda + 2\mu)d_n\, \tau_B$	Bulk-free carrier lifetime
ϑ, $\left(\dot{\vartheta} = \theta\right)$	Thermal displacement
D_E	Ambipolar diffusion parameter
$\overrightarrow{J}$	Current density
ε_0	Electric permeability

1 Introduction

Renewable energy sources are driving the use of naturally occurring materials in many sectors. In solar cell technology, for instance, semiconductor materials are essential but costly. However, recent advances have shown that these materials can be excited by a laser or sunlight to stimulate surface electrons, making them more economically viable [1]. Optical excitation of short elastic pulses has also become a crucial area of study for engineers and physicists, particularly in fields such as laser engraving, photoacoustic microscopy, and image formation by thermal waves. While many studies have explored the effects of thermoplastic and electronic deformations on semiconductor media, few have considered their relationship with plasma interactions and thermoelasticity [2, 3]. The depth dependence of plasma waves generates both thermal and elastic waves, leading to periodic changes in temperature and mechanical oscillation. Thermoelastic coupling results from heat waves propagating elastic oscillations toward the surface in a feedback loop where the energy released from heating a material causes an elastic wave to propagate, releasing more heat. Photogenerated carriers in semiconductors cause periodic elastic distortions called electron distortions (ED) [4].

Theoretical analysis of transport characteristics and carrier recombination in semiconductor media has been explored by Todorovic [5, 6] and Song et al. [7]. Recent shifts in thermal and plasma wave propagation are due to the linear relationship between thermal and mass transport. When laser beams hit flexible semiconductors, high-frequency elastic waves are generated that cause internal elastic components to vibrate, resulting in wave propagation and the release of electrons. For instance, photoexcited electrons may generate plasma waves, whose charge intensity can be quantified. The study of plasma, thermal, and elastic model systems, as well as the thermoelastic and electrical deformation impacts in semiconductor materials, has been the subject of research by many scholars [8–14].

Thermoelasticity refers to how temperature changes affect the volume and shape of solids. Materials with higher elasticity will stretch and shrink more easily than those with lower elasticity. Understanding thermoelasticity is crucial for creating materials and devices that can withstand temperature fluctuations without breaking. The field of engineering offers ample opportunities to harness the benefits of extended thermoelasticity, from

soil dynamics and oil extraction to mineral discovery and earthquake prediction. Despite the fact that scientists have known the equations describing thermoelasticity for over a century, it is only recently that stress testing materials has been utilized to determine their thermoelastic properties. By subjecting materials to varying temperatures, engineers can estimate how much they will expand or contract. This information is vital for building machinery or load-bearing structures with components that must fit together precisely. Engineers can improve the thermal stability of products by understanding the fundamentals of thermoelasticity.

Feng et al. [15] developed sandwich composites inspired by nature to dampen vibrations, and conducted a comparative study involving samples made from traditional composites and pure epoxy resin. Dynamic mechanical examination and vibration tests revealed that sandwich composites outperformed combined composites and pure epoxy in terms of damping qualities. Safaei et al. [16] explored honeycomb sandwich constructions with varying boundary conditions, performing free vibration, modal, and stress state studies and identifying key influences on sandwich frequencies and stiffness due to changes in materials or parameters. Sarkon et al. [17] discussed cutting-edge machine learning techniques with practical applications in additive manufacturing, evaluating how various methods and designs are typically categorized. İnada et al. [18] focused on nanomaterials and the parameters determining their effectiveness in energy storage and conversion, investigating efficient materials used in solar energy conversion and storage systems. Alhijazi et al. [19] investigated the impact of changing fiber volume fractions (Vf) on the elastic characteristics of natural fiber composites (NFC) made from Luffa and Palm in high-density polyethylene (HDPE) and polypropylene (PP) matrices.

The system of equations governing the displacement–temperature domain is hyperbolic-parabolic, but it contradicts experimental results because the reaction of a thermoelastic body to thermomechanical stress propagates at an infinitely rapid rate over long distances. To address this issue, several theories have been proposed since 1967, all of which are known as generalized thermoelasticity models. One such theory is the extended thermoelastic theory with single-phase lag, developed by Lord and Shulman [20]. This theory led to the development of a new law of heat transfer, which has replaced the traditional Fourier law. The extended thermoelastic model with two relaxation times, introduced by Green and Lindsay [21], gained widespread attention. Tzou [22] investigated the process of heat conduction from its undetectable to its observable extent and proposed the dual-phase lag hypothesis, which is supported by both experimental and analytical evidence [23]. Green developed his thermoelastic models [24–26] to provide an explanation that accounts for both flexible and heat transfer waves connected to second sound. Many publications have examined thermoelasticity from theoretical and empirical perspectives, often focusing on type II or III of Green-Naghdi types. Choudhuri [27] presented the three-phase delay thermoelasticity concept based on the ideas created by Green and Naghdi [24].

Several scientific researches in recent years have discussed the Moore-Gibson-Thompson (MGT) equation and its various interpretations. This equation is based on ubiquitous third-order differential equations used extensively in fluid dynamics [28]. The MGT equation has found applications in many fields, including high-intensity ultrasound lithotripsy, thermotherapy, ultrasonic cleaning, among others. Quintanilla [29, 30] has been designing a novel thermoelasticity system for MGT thermal transmission. Additionally, Abouelregal et al. [31–34] constructed an updated heat transport equation by adding the relaxation component to the GN-III system and using the energy equation. This updated heat transport equation is highly recommended.

Semiconductor physics is a rapidly developing subfield in materials science and solid-state physics. The micro- and nanostructures of semiconductor technology experience plasma, thermal, elastic, and acoustic phenomena, which pose significant challenges to modern semiconductor physics and technologies. Updated models of featuring pulsed lasers have shown great potential in stimulating and processing various materials, making them valuable tools for scientific research. Apart from this, lasers are also widely used in several other professions and industries, such as medicine and manufacturing. Laser technologies enable laser burning, cutting, and engraving, as well as optical material spectroscopy and dynamic combustion research. Some notable applications of these laser-based technologies include:

The aim of the present study is to introduce a system of photothermal equations that describe the behavior of photo- and thermo-carriers in semiconductor materials when excited by strong femtosecond laser pulses. The proposed model, referred to as 4MGT-PTE, builds upon Green and Naghdi's third-type models [14–16] and incorporates MGT's idea of fourth-order time derivatives for the first time. By including the thermal relaxation factor before the time derivatives of the third and fourth orders, this structure allows the transmission of heat waves at a maximum finite speed and extends the theory of isotropic materials. To the best of the authors' knowledge, the fourth-order version of photo-thermoelasticity, namely 4MGT-PTE, has not been used previously to investigate the spread of photothermal waves in semiconductor materials. This paper discusses various types of optically stimulated plasmas, as well as plasmonic phenomena and thermoelastic semiconductor structures.

2 Conceptualization and basic equations

When conducting theoretical assessments of the transfer process in semiconductor materials, it is common practice to account for coupled plasma, thermal, and elastic waves. For isotropic and homogeneous materials, the constitutive relations and equations governing plasma, elastic, and thermal transport can be expressed as [6, 7, 35]:

$$(\lambda+\mu)\nabla(\nabla\cdot\vec{\mathrm{u}})+\mu\nabla^2\vec{\mathrm{u}}+\vec{\mathrm{F}}=\rho\frac{\partial^2\vec{\mathrm{u}}}{\partial t^2}+\gamma_\theta\nabla\theta+\gamma_n\nabla N \tag{1}$$

$$\left(D_E\nabla^2-\rho\frac{\partial}{\partial t}-\frac{1}{\tau_B}\right)N=\kappa\theta \tag{2}$$

$$2e_{ij}=u_{i,j}+u_{j,i} \tag{3}$$

$$\overline{\overline{\sigma}}=\lambda(\nabla\cdot\vec{u})\overline{\overline{I}}+\mu\left(\nabla\vec{u}+\nabla\left(\vec{u}^{\mathrm{Tr}}\right)\right)-(\gamma_\theta\theta+\gamma_n N)\overline{\overline{I}} \tag{4}$$

$$\rho C_E\frac{\partial\theta}{\partial t}+\gamma_\theta T_0\frac{\partial}{\partial t}(\nabla\cdot\vec{\mathrm{u}})=-\vec{\nabla}\cdot\vec{H}+Q \tag{5}$$

$$\vec{H}\left(\vec{X},t\right)=-K\,\vec{\nabla}\theta-K^*\vec{\nabla}\vartheta-\int\frac{E_{\mathrm{g}}}{\tau_{\mathrm{B}}}N d\vec{X} \tag{6}$$

where $\overline{\overline{\sigma}}$ is the stress tensor and $\overline{\overline{I}}$ is the identity tensor.

The assumption that the heat transfer waves will move at a finite rate is shown to be unrealistic when using the conservation Eqs. (5) in combination with the modified Fourier law of the Green and Naghdi models (GN-III), as defined by Eq. (6). Because of this, adding variables for delay or relaxation to the above equations seems like an excellent way to fine-tune this theory.

The Taylor series approximation can be used to determine the heat flow $\overrightarrow{H}$ when the phase delay (τ_q) is considered. In this context, the heat flux $\overrightarrow{H}$ can be then expressed as:

$$\vec{H}\left(\vec{X},t+\tau_q\right)\approx\vec{H}\left(\vec{X},t\right)+\tau_q\frac{\partial\vec{H}\left(\vec{X},t\right)}{\partial t}+\frac{1}{2}\tau_q^2\frac{\partial^2\vec{H}\left(\vec{X},t\right)}{\partial t^2} \tag{7}$$

By substituting Eq. (7) into Eq. (6), one can derive the new photothermal MGT Fourier law:

$$\vec{H}\left(\vec{X},t\right)+\tau_q\frac{\partial\vec{H}\left(\vec{X},t\right)}{\partial t}+\frac{1}{2}\tau_q^2\frac{\partial^2\vec{H}\left(\vec{X},t\right)}{\partial t^2}=-\left[K\,\vec{\nabla}\theta+K^*\vec{\nabla}\vartheta+\int\frac{E_{\mathrm{g}}}{\tau_{\mathrm{B}}}N\mathrm{d}\vec{X}\right] \tag{8}$$

Differentiating the previous equation with respect to the position vector $\overrightarrow{X}$ will result in:

$$\vec{H}\left(\vec{X},t\right)+\tau_q\frac{\partial\vec{H}\left(\vec{X},t\right)}{\partial t}+\frac{1}{2}\tau_q^2\frac{\partial^2\vec{H}\left(\vec{X},t\right)}{\partial t^2}=-\left(\left(K\frac{\partial}{\partial t}+K^*\right)\vec{\nabla}\theta+\frac{E_{\mathrm{g}}}{\tau_{\mathrm{B}}}\frac{\partial N}{\partial t}\right) \tag{9}$$

We derive the modified fourth-order MGT photothermal heat transfer equation by inserting Eq. (9) into the energy Eq. (5) as follows:

$$\begin{aligned}\left(1+\tau_q\tfrac{\partial}{\partial t}+\tfrac{1}{2}\tau_q^2\tfrac{\partial^2}{\partial t^2}\right)\tfrac{\partial}{\partial t}\left[\rho C_E\tfrac{\partial\theta}{\partial t}+\gamma_\theta T_0\tfrac{\partial}{\partial t}\left(\vec{\nabla}\cdot\vec{u}\right)-Q\right]\\=\nabla.\left(K\,\nabla\dot{\theta}\right)+\nabla.(K^*\nabla\theta)+\tfrac{E_{\mathrm{g}}}{\tau_{\mathrm{B}}}\tfrac{\partial N}{\partial t}\end{aligned} \tag{10}$$

The interaction between thermal-plasma-elastic waves is explained by this equation. However, it has been observed that internal friction plays a significant role in attenuation and scattering of these waves. Therefore, understanding the viscoelastic behavior of materials is crucial for accurately modeling wave propagation processes. Several theoretical frameworks have been developed to account for energy dissipation in vibrating solids due to viscoelasticity. Knowledge about viscoelastic behavior is particularly relevant in the field of engineering materials, where certain materials exhibit viscoelastic interaction with stress [36]. This area of research has important implications in fields such as materials science, mineralogy, and solid-state physics.

To this end, the Kelvin–Voigt concept of linear viscoelasticity is utilized to characterize the viscoelastic features of isotropic materials. When the influence of viscosity is considered, the values for the coefficients λ, μ, γ_θ, and γ_n are as follows [37]:

$$\begin{aligned} \lambda =&\lambda_{\mathrm{e}} + \alpha_1 \lambda_{\mathrm{e}} \frac{\partial}{\partial t}, \ \mu = \mu_{\mathrm{e}} + \alpha_2 \mu_{\mathrm{e}} \frac{\partial}{\partial t}, \\ \gamma_\theta =&\gamma_{1\mathrm{e}} + \alpha_3 \gamma_{1\mathrm{e}} \frac{\partial}{\partial t}, \gamma_n = \gamma_{2\mathrm{e}} + \alpha_4 \gamma_{2\mathrm{e}} \frac{\partial}{\partial t}, \end{aligned} \tag{11}$$

where

$$\begin{aligned} \gamma_{1\mathrm{e}} =&(3\lambda_{\mathrm{e}} + 2\mu_{\mathrm{e}})\alpha_t, \ \ \alpha_3 = (3\lambda_{\mathrm{e}}\alpha_1 + 2\mu_{\mathrm{e}}\alpha_2)\alpha_{\mathrm{t}}/\gamma_{1\mathrm{e}} \\ \gamma_{2\mathrm{e}} =&(3\lambda_{\mathrm{e}} + 2\mu_{\mathrm{e}})d_n, \ \ \alpha_4 = (3\lambda_{\mathrm{e}}\alpha_1 + 2\mu_{\mathrm{e}}\alpha_2)d_n/\gamma_{2\mathrm{e}} \end{aligned} \tag{12}$$

3 Electromagnetic Maxwell's equations

Maxwell's equations helped us understand that light is actually made up of an electromagnetic field. This field follows the wave equation and travels at the speed of light through empty space. In a vacuum, electromagnetic waves are transverse because the electric and magnetic fields are always perpendicular to the direction of the wave's movement. If there's no electric or magnetic field present, then no electromagnetic waves will be sent out. When any physical process involves both temperature and electromagnetic fields together, it is called "thermo-electromagnetism". Because an oscillating electric field $\overrightarrow{\mathrm{H}}$ creates an oscillating magnetic field $\overrightarrow{\mathrm{h}}$, which in turn produces an oscillating electric field $\overrightarrow{\mathrm{E}}$, Maxwell's equations predicted that electricity and magnetism would act like electromagnetic waves. The equations of Maxwell may be rewritten using the differential form as follows [38, 39]:

$$\begin{aligned} \vec{J} + \varepsilon_0 \frac{\partial \vec{E}}{\partial t} =&\nabla \times \vec{h}, \quad \times \vec{E} + \frac{\partial \vec{B}}{\partial t} = 0, \quad \vec{E} + \left(\frac{\partial \vec{u}}{\partial t} \times \vec{B} \right) = 0, \\ \vec{B} =&\mu_0 \left(\vec{H} + \vec{h} \right), \quad \nabla \cdot \vec{h} = 0. \end{aligned} \tag{13}$$

There is a relationship between electromagnetic forces and mechanical momentum, and the Maxwell stress tensor represents this correlation. The stress tensor M_{ij} of the electromagnetic field, known as the Maxwell stress tensor, can be expressed by the following formula:

$$M_{ij} = \mu_0 \left[H_i h_j + H_j h_i - H_k h_k \delta_{ij} \right] \tag{14}$$

In an electric field $\vec{\mathrm{E}}$ and a magnetic field $\vec{\mathrm{H}}$, a charged particle q_e traveling at speed $\frac{\partial \vec{\mathrm{u}}}{\partial t}$ experiences the Lorentz force $\vec{\mathrm{F}}$. The Lorentz force $\vec{\mathrm{F}}$ exerted on the charged particle is then given by:

$$\vec{\mathrm{F}} = \mu_0 \left(\nabla \times \vec{\mathrm{H}} \right) \tag{15}$$

4 Statement of the problem

This investigation considers a two-dimensional photo-elastic thermoelastic medium (half-space) in which the free surface penetrates the solid along the x-axis. At time $t = 0$, the surface layer ($x = 0$) is supposed to be heated by a thermal flux in the form of a fast laser pulse. It will be taken into account that the force perpendicular to the body's surface ($x = 0$) depends on the time t and the Cartesian coordinates x and z. This is because the laser pulses cause heating in a direction perpendicular to the oxz plane. When x reaches infinity, all physical fields will diminish to the point of vanishing away from the surface; thus, the conditions for uniformity will be considered.

The following expression can represent the displacement component in x and z directions:

$$\vec{\mathrm{u}} \equiv (u(x, z, t), \ 0, \ w(x, z, t)) \tag{16}$$

This equation enables us to determine the dilatation (e) as:

$$e(x,z,t) = \mathrm{div}(\vec{\mathrm{u}}) = \frac{\partial u}{\partial x} + \frac{\partial w}{\partial z} \tag{17}$$

After exposing the surface to an initial magnetic field $\vec{\mathrm{H}}_0 = (0,\ H_0,\ 0)$, the Lorentz force $\vec{\mathrm{F}}$ is given by:

$$F_x = \left(\mu_0 H_0^2 \frac{\partial e}{\partial x} - \varepsilon_0 \mu_0^2 H_0^2 \frac{\partial^2 u}{\partial t^2}\right),\ F_y = 0,\ F_z = \left(\mu_0 H_0^2 \frac{\partial e}{\partial z} - \varepsilon_0 \mu_0^2 H_0^2 \frac{\partial^2 w}{\partial t^2}\right) \tag{18}$$

In Eq. (1), for x and z axes, the following formulas are used when the Lorentz force is taken into consideration:

$$\left(\lambda + \mu + \mu_0 H_0^2\right)\frac{\partial e}{\partial x} + \left(\mu\nabla^2 - \left(\rho + \varepsilon_0 \mu_0^2 H_0^2\right)\frac{\partial^2}{\partial t^2}\right)u = \frac{\partial}{\partial x}(\gamma_\theta \theta + \gamma_n N) \tag{19}$$

$$\left(\lambda + \mu + \mu_0 H_0^2\right)\frac{\partial e}{\partial z} + \left(\mu\nabla^2 - \left(\rho + \varepsilon_0 \mu_0^2 H_0^2\right)\frac{\partial^2}{\partial t^2}\right)w = \frac{\partial}{\partial z}(\gamma_\theta \theta + \gamma_n N) \tag{20}$$

By utilizing Eq. (17) and eliminating u and w from Eqs. (19) and (20), we can derive the following equation:

$$\left[\left(\frac{\lambda_\mathrm{e} + 2\mu_\mathrm{e}}{\rho} + \frac{\lambda_\mathrm{e}\alpha_1 + 2\mu_\mathrm{e}\alpha_2}{\rho}\frac{\partial}{\partial t} + \frac{\mu_0 H_0^2}{\rho}\right)\nabla^2 - \left(1 + \varepsilon_0 \mu_0^2 H_0^2\right)\frac{\partial^2}{\partial t^2}\right]e = \frac{1}{\rho}\nabla^2(\gamma_\theta \theta + \gamma_n N) \tag{21}$$

It is possible to write the coupled plasma wave Eq. (2) as follows:

$$\left[D_E\left(\frac{\partial^2}{\partial x^2} + \frac{\partial^2}{\partial z^2}\right) - \rho\frac{\partial}{\partial t} - \frac{1}{\tau_B}\right]N = \kappa\theta \tag{22}$$

In addition, the proposed fourth-order MGT photothermal model may be reformulated when there is no heat source, as follows:

$$\left(1 + \tau_q\frac{\partial}{\partial t} + \frac{1}{2}\tau_q^2\frac{\partial^2}{\partial t^2}\right)\frac{\partial^2}{\partial t^2}(\rho C_E\theta + \gamma T_0 e) = \left(K^* + K\frac{\partial}{\partial t}\right)\left(\frac{\partial^2}{\partial x^2} + \frac{\partial^2}{\partial z^2}\right)\theta + \left(E_\mathrm{g}/\tau_\mathrm{B}\right)\frac{\partial N}{\partial t} \tag{23}$$

The four constitutive equations may be written in x, y, and z directions as follows:

$$\begin{aligned}
\sigma_{xx} =& \left(\lambda_\mathrm{e} + \alpha_1\lambda_\mathrm{e}\frac{\partial}{\partial t}\right)\frac{\partial w}{\partial z} + (\lambda_\mathrm{e} + 2\mu_\mathrm{e})\left(1 + \frac{\lambda_\mathrm{e}\alpha_1 + 2\mu_\mathrm{e}\alpha_2}{\lambda_\mathrm{e} + 2\mu_\mathrm{e}}\frac{\partial}{\partial t}\right)\frac{\partial u}{\partial x} - (\gamma_\theta\theta + \gamma_n N)\\
\sigma_{zz} =& \left(\lambda_\mathrm{e} + \alpha_1\lambda_\mathrm{e}\frac{\partial}{\partial t}\right)\frac{\partial u}{\partial x} + (\lambda_\mathrm{e} + 2\mu_\mathrm{e})\left(1 + \frac{\lambda_\mathrm{e}\alpha_1 + 2\mu_\mathrm{e}\alpha_2}{\lambda_\mathrm{e} + 2\mu_\mathrm{e}}\frac{\partial}{\partial t}\right)\frac{\partial w}{\partial z} - (\gamma_\theta\theta + \gamma_n N)\\
\sigma_{xz} =& \left(\mu_\mathrm{e} + \alpha_2\mu_\mathrm{e}\frac{\partial}{\partial t}\right)\left(\frac{\partial u}{\partial z} + \frac{\partial w}{\partial x}\right)
\end{aligned} \tag{24}$$

It is common to include the non-dimensional variables expressed by:

$$\begin{gathered}
\left\{x', z'\right\} = \tfrac{\eta_0\{x,z\}}{c_0},\ \ \left\{u', w'\right\} = \tfrac{\eta_0\{u,w\}}{c_0},\ \ \left\{\theta', N'\right\} = \tfrac{1}{\rho c_0^2}\{\gamma_{1e}\theta, \gamma_{2e}N\},\\
t' = \eta_0 t,\ \ \tau_q = \eta_0\tau_q,\ \ \sigma'_{ij} = \sigma_{ij}/(\gamma_{1e}T_0),\ \ \eta_0 = \rho C_E c_0^2/K,\ \ c_0^2 = c_1^2 + a_0^2,
\end{gathered} \tag{25}$$

where $c_1^2 = (\lambda_e + 2\mu_e)/\rho$, $c_2^2 = \mu_e/\rho$, and $a_0^2 = \mu_0 H_0^2/\rho$.

After introducing the dimensionless expressions specified by Eq. (25), the finalized Eqs. (21)-(23) have the following forms by removing the prime symbols:

$$\left[\left(1 + \frac{\lambda_e\alpha_1 + 2\mu_e\alpha_2}{\rho c_1^2}\frac{\partial}{\partial t} + a_0^2\right)\nabla^2 - g_0\frac{\partial^2}{\partial t^2}\right]e = \nabla^2\left[\left(1 + \alpha_3\frac{\partial}{\partial t}\right)\theta + \left(1 + \alpha_4\frac{\partial}{\partial t}\right)N\right] \tag{26}$$

$$\begin{aligned}
&\left(1 + \tau_q\frac{\partial}{\partial t} + \frac{1}{2}\tau_q^2\frac{\partial^2}{\partial t^2}\right)\frac{\partial^2}{\partial t^2}\left(\theta + \varepsilon_1\left(1 + \alpha_3\frac{\partial}{\partial t}\right)e\right)\\
&\qquad = \left(\overline{K}^* + \frac{\partial}{\partial t}\right)\left(\frac{\partial^2\theta}{\partial x^2} + \frac{\partial^2\theta}{\partial z^2}\right) + \varepsilon_2\frac{\partial N}{\partial t}
\end{aligned} \tag{27}$$

$$\left[\left(1+\alpha_4\frac{\partial}{\partial t}\right)\left(\frac{\partial^2}{\partial x^2}+\frac{\partial^2}{\partial z^2}\right)-g_1\left(1+\alpha_4\frac{\partial}{\partial t}\right)\frac{\partial}{\partial t}-g_2\left(1+\alpha_4\frac{\partial}{\partial t}\right)\right]N=g_3\left(1+\alpha_3\frac{\partial}{\partial t}\right)\theta \tag{28}$$

where

$$\begin{gathered}\varepsilon_1=(\gamma_{1e})^2T_0/\left(\rho^2C_Ec_0^2\right),\ \ \varepsilon_2=\gamma_{1e}E_g\eta_0/(\tau_B\rho C_E\gamma_{2e}),\overline{K}^*=K^*/\left(c_0^2K\rho\right),\\ g_0=1+\mu_0\varepsilon_0a_0^2,g_1=\rho c_0^2/(\eta_0D_E),g_2=c_0^2/(\tau_BD_E),g_3=\frac{\kappa c_0^2\gamma_{2e}}{\eta_0^2D_E}\end{gathered} \tag{29}$$

Thereby, Eq. (24) take the following forms when the non-dimensional quantities are applied:

$$\begin{aligned}\sigma_{xx}&=\left(C_{11}+C_{14}\frac{\partial}{\partial t}\right)\frac{\partial u}{\partial x}+C_{12}\left(1+\alpha_1\frac{\partial}{\partial t}\right)\frac{\partial w}{\partial z}-\left(1+\alpha_3\frac{\partial}{\partial t}\right)\theta-\left(1+\alpha_4\frac{\partial}{\partial t}\right)N\\ \sigma_{zz}&=\left(C_{11}+C_{14}\frac{\partial}{\partial t}\right)\frac{\partial w}{\partial z}+C_{12}\left(1+\alpha_1\frac{\partial}{\partial t}\right)\frac{\partial u}{\partial x}-\left(1+\alpha_3\frac{\partial}{\partial t}\right)\theta-\left(1+\alpha_4\frac{\partial}{\partial t}\right)N\\ \sigma_{xz}&=C_{13}\left(1+\alpha_2\frac{\partial}{\partial t}\right)\left(\frac{\partial u}{\partial z}+\frac{\partial w}{\partial x}\right)\end{aligned} \tag{30}$$

where

$$C_{11}=\frac{\lambda_e+2\mu_e}{c_1^2+a_0^2},C_{12}=\frac{\lambda_e}{c_1^2+a_0^2},C_{13}=\frac{\mu_e}{c_1^2+a_0^2},C_{14}=\frac{\lambda_e\alpha_1+2\mu_e\alpha_2}{c_1^2+a_0^2}. \tag{31}$$

5 Normal mode technique

To deal with the governing partial differential equations derived in this study, different numerical and semi-analytical methods introduced in the literature can be employed [40–47]. In this section, the following expressions are utilized in order to calculate the solutions in the context of normal modes:

$$\left\{u,\ w,\ \theta,\ e,\ N,\ \sigma_{ij}\right\}(x,z,t)=\left\{u^*,\ w^*,\ \theta^*,\ e^*,\ N^*,\ \sigma_{ij}^*\right\}(x)\mathrm{Exp}(iaz+\omega t) \tag{32}$$

where the variables $u^*(x)$, $w^*(x)$, $\theta^*(x)$, $\mathrm{e}^*(x)$, $N^*(x)$, and $\sigma_{ij}^*(x)$ denote the magnitudes of the photo-thermophysical variables. In addition, $i=\sqrt{-1}$, and the symbol a represents the wavenumber in z direction, and ω represents the frequency. The results of applying the normal mode method on the governing Eqs. (26)–(30) are as follows:

$$\left(\frac{\mathrm{d}^2}{\mathrm{d}x^2}-\zeta_1\right)\mathrm{e}^*=\left(\frac{\mathrm{d}^2}{\mathrm{d}x^2}-a^2\right)\left[\delta_0\theta^*+\delta_1N^*\right] \tag{33}$$

$$\left(\frac{\mathrm{d}^2}{\mathrm{d}x^2}-\zeta_3\right)N^*=\delta_3\theta^* \tag{34}$$

$$\delta_4\mathrm{e}^*-\delta_5N^*=\left(\frac{\mathrm{d}^2}{\mathrm{d}x^2}-\zeta_2\right)\theta^* \tag{35}$$

$$\begin{aligned}\sigma_{xx}^*&=\Omega_1\frac{\mathrm{d}u^*}{\mathrm{d}x}+ia\Omega_2w^*-\Omega_4\theta^*-\Omega_5N^*\\ \sigma_{zz}^*&=ia\Omega_1w^*+\Omega_2\frac{\mathrm{d}u^*}{\mathrm{d}x}-\Omega_4\theta^*-\Omega_5N^*\\ \sigma_{xz}^*&=\Omega_3\left(iau^*+\frac{\mathrm{d}w^*}{\mathrm{d}x}\right)\end{aligned} \tag{36}$$

where

$$\begin{aligned}&\zeta_1=a^2+\frac{\rho c_1^2g_0\omega^2}{\rho c_1^2+\omega\left(\lambda_e\alpha_1+2\mu_e\alpha_2++\mu_0H_0^2\right)},\ \ q=\frac{\omega^2\left(1+\tau_q\omega+\frac{1}{2}\tau_q^2\omega^2\right)}{\overline{K}^*+\omega},\\ &\zeta_2=a^2+q,\delta_1=\frac{\rho c_1^2(1+\alpha_3\omega)}{\rho c_1^2+\omega(\lambda_e\alpha_1+2\mu_e\alpha_2)},\ \ \delta_2=\frac{\rho c_1^2(1+\alpha_4\omega)}{\rho c_1^2+\omega(\lambda_e\alpha_1+2\mu_e\alpha_2)},\ \ \delta_3=\frac{g_3(1+\alpha_3\omega)}{1+\alpha_4\omega}\\ &\zeta_3=a^2+g_1\omega+g_2,\ \ \delta_4=q\varepsilon_1(1+\alpha_3\omega),\ \ \delta_5=\omega\varepsilon_2(1+\alpha_4\omega),\ \ \Omega_1=C_{11}+C_{14}\omega,\end{aligned}$$

$$\Omega_2 = C_{12}(1+\alpha_1\omega),\quad \Omega_3 = C_{13}(1+\alpha_2\omega),\quad \Omega_4 = (1+\alpha_3\omega),\quad \Omega_5 = (1+\alpha_3\omega). \tag{37}$$

By considering Eqs. (33)–(36), one can deduce the following expression for e^*:

$$\left(\frac{\mathrm{d}^6}{\mathrm{d}x^6} - A\frac{\mathrm{d}^4}{\mathrm{d}x^4} + B\frac{\mathrm{d}^2}{\mathrm{d}x^2} - C\right)e^* = 0, \tag{38}$$

with

$$\begin{gathered} \mathrm{D} = \frac{\mathrm{d}u}{\mathrm{d}x},\ A = \zeta_3 + g_5,\quad B = \zeta_3 g_5 + g_6 - \delta_3 g_7,\quad C = \zeta_3 g_6 + \delta_3 g_8, \\ g_5 = \zeta_1 + \zeta_2 + \delta_0\delta_4,\quad g_6 = \zeta_1\zeta_2 + \delta_0\delta_4 a^2, g_7 = \delta_1\delta_4 - \delta_5, g_8 = \zeta_1\delta_5 - a^2. \end{gathered} \tag{39}$$

It is possible to factor Eq. (38) by using:

$$\left(\frac{\mathrm{d}^2}{\mathrm{d}x^2} - k_1^2\right)\left(\frac{\mathrm{d}^2}{\mathrm{d}x^2} - k_2^2\right)\left(\frac{\mathrm{d}^2}{\mathrm{d}x^2} - k_3^2\right)e^* = 0, \tag{40}$$

Following is a polynomial function that may be solved to obtain the variables k_n^2, $n = 1, 2, 3$, respectively:

$$k^6 - Ak^4 + Bk^2 - C = 0. \tag{41}$$

The analysis disregards the physical issue of positive exponent to satisfy the uniformity criterion. This will ensure us that the solution of the problem does not diverge as they approach to infinity. The solution of Eq. (40), which considers a restriction when $x \to \infty$, may be introduced as:

$$e^*(x) = \sum_{n=1}^{3} C_n \mathrm{e}^{-k_n x}. \tag{42}$$

The same approach may be used to obtain the following solutions as well:

$$\left\{N^*, \theta^*\right\}(x) = \sum_{n=1}^{3}\left\{C_n', C_n''\right\}e^{-k_n x}, \tag{43}$$

where the parameters C_n' and C_n'' are independent. Inserting Eqs. (42) and (43) into Eqs. (34) and (35) leads to:

$$C_n'(a,\omega) = H_n C_n, C_n''(a,\omega) = L_n C_n(a,\omega), \tag{44}$$

where

$$H_n = \frac{\delta_3\delta_4}{\left(k_n^2 - \zeta_2\right)\left(k_n^2 - \zeta_3\right) + \delta_3\delta_5}, L_n = \frac{\left(k_n^2 - \zeta_3\right)H_n}{\delta_3}. \tag{45}$$

After introducing the non-dimensional parameters defined in (32), we obtain the following from Eqs. (42) and (43):

$$\left(\frac{\mathrm{d}^2}{\mathrm{d}x^2} - k_4^2\right)u^* = \sum_{n=1}^{3} C_n M_n \mathrm{e}^{-k_n x} \tag{46}$$

where

$$\begin{aligned} M_n &= \frac{k_n\left(\left(\rho c_1^2 + (\lambda_e\alpha_1 + \mu_e\alpha_2)\omega + \rho c_1^2 a_0^2\right) - \rho c_1^2(1+\alpha_3\omega)L_n - \rho c_1^2(1+\alpha_4\omega)H_n\right)}{c_2^2(1+\alpha_3\omega)} \\ k_4^2 &= a^2 + \frac{\rho c_1^2\omega^2 g_0}{c_2^2(1+\alpha_3\omega)}, \end{aligned} \tag{47}$$

It is possible to achieve the following result in light of the regularity criterion:

$$u^* = \sum_{n=1}^{3}\left\{\frac{M_n}{k_n^2 - k_4^2}C_n\right\}\mathrm{e}^{-k_n x} + C_4\mathrm{e}^{-k_4 x} \tag{48}$$

Thereby, the solution form of w^* can be written by:

$$w^* = \frac{1}{ia}\sum_{n=1}^{3}\left(\frac{k_n M_n}{k_n^2 - k_4^2} + 1\right)C_n e^{-k_n x} + \frac{C_4 k_4}{ia}e^{-k_4 x} \tag{49}$$

As a result of inserting the obtained solutions (u^*, w^*, N^* and θ^*) into Eq. (36), one can calculate the thermal stresses as:

$$\begin{aligned}
\sigma_{xx}^* &= \sum_{n=1}^{3} C_n R_n e^{-k_n x} + R_4 C_4 e^{-k_4 x} \\
\sigma_{zz}^* &= \sum_{n=1}^{3} C_n Q_n e^{-k_n x} + Q_4 C_4 e^{-k_4 x} \\
\sigma_{xz}^* &= \sum_{n=1}^{3} C_n P_n e^{-k_n x} + C_4 P_4 e^{-k_4 x}
\end{aligned} \tag{50}$$

where

$$\begin{aligned}
R_n &= \frac{k_n C_{12} M_n}{k_n^2 - k_4^2} + \frac{k_n C_{11} M_n}{-k_n^2 + k_4^2} - (H_n + L_n) + 1, \quad R_4 = k_4 C_{12} - k_4 C_{11}, \\
Q_n &= \frac{k_n C_{11} M_n}{k_n^2 - k_4^2} + \frac{k_n C_{12} M_n}{-k_n^2 + k_4^2} - (H_n + L_n) + 1, \quad Q_4 = k_4 C_{11} - k_4 C_{12}, \\
P_n &= -\frac{C_{13} M_n\left(a^2 + k_n^2\right)}{ia\left(k_n^2 - k_4^2\right)} + \frac{k_n^2 C_{13}}{ia}, \quad P_4 = -\frac{a^2 C_{13}}{ia} - \frac{k_4^2 C_{13}}{ia}.
\end{aligned} \tag{51}$$

6 Applications

The unknown parameters C_j, where $j = 1, 2, 3$, and 4, will be set in this section. It must be considered that the initial conditions of the suggested problem require that the medium is initially at rest where there is no deformation or stress. It will be taken into account that there is a force P depends on both time and spatial coordinates z acting on the medium at the surface $x = 0$. On the surface $x = 0$, the following mechanical boundary conditions apply:

$$\sigma_{zz}(x, z, t) = -P, \quad \sigma_{xz}(x, z, t) = 0 \text{ at } x = 0. \tag{52}$$

Various physical phenomena may occur when a laser beam is applied to an elastic surface, some of which are sensitive to the incident power. Since high incident forces damage the material's surface, this method is unsuitable for non-destructive testing and will only be addressed at low incident level. The laser source generates heat; thermal waves are created due to heat transfer, and elastic waves are produced at low incidence powers. Materials like semiconductors have the potential to conduct electricity when the right conditions are precisely met. It is considered that the plane surrounding the thermoelastic medium ($x = 0$) is subject to thermal shocks in the form of laser pulses. Therefore, in this scenario, the following thermal conditions can be taken into account [48]:

$$\theta(x, z, t) = \frac{16\hat{E}\hat{\gamma}\left(1 - \hat{R}\right)}{R_G v^4\sqrt{2\pi}} e^{-2z^2/R_G} t^3 e^{-2t^2/v^2} \tag{53}$$

For the purpose of laser heating of metals, it is helpful to assume a surface source, as demonstrated in Eq. (52), in which $\widehat{E}$ is the energy of the laser pulse per unit length, $\widehat{R}$ is the surface reflectivity, R_G is the radius of the Gaussian beam, v is the rise time of the laser pulse, and $\widehat{\gamma}$ is the extinction coefficient. During one stage, a laser can produce the maximum amount of light energy $\widehat{E}$. Due to the fact that the light energy is defined by a Gaussian in z direction, Eq. (53) represents an illumination strip.

The impact of surface recombination on device characteristics is widely recognized. Devices with a high ratio of surface area to volume can be particularly affected, with surface recombination dominating their features. As time progresses, carriers diffuse toward the sample's surface and have a predetermined probability of undergoing recombination. Whether the process is carried out optically or thermally, recombination and

generation are constant processes that occur in semiconductors. Thermodynamically speaking, when a substance reaches thermal equilibrium, its generation and recombination rates will reach an equilibrium state. This ensures that the total charge carrier density remains constant. Hence, the following expression can be utilized to describe the carrier density boundary condition:

$$D_E \left.\frac{\partial N}{\partial x}\right|_{x=0} = s_{\mathrm{f}} N(0,z,t), \tag{54}$$

where s_{f} is the rate of recombination close to the surface, it is common practice to discuss the surface recombination velocities when discussing carrier distributions close to a surface.

By inserting the solutions of the relevant variables into the boundary conditions mentioned above, one gets the following equations for the parameters C_j, where $j = 1, 2, 3, 4$:

$$\begin{Bmatrix} C_1 \\ C_2 \\ C_3 \\ C_4 \end{Bmatrix} = \begin{bmatrix} R_1 & R_2 & R_3 & R_4 \\ P_1 & P_2 & P_3 & P_4 \\ G_1 & G_2 & G_3 & 0 \\ L_1 & L_2 & L_3 & 0 \end{bmatrix}^{-1} \begin{Bmatrix} -P_0 \\ 0 \\ 0 \\ P_1 \end{Bmatrix}. \tag{55}$$

where $G_n = H_n\left(D_E k_n + s_f\right)$

After utilizing the inverse matrix method, it is possible to acquire the values of the four unknown coefficients C_j, where $j = 1, 2, 3$, and 4. Consequently, the solutions are obtained for the thermal deformations, the temperature change, and other photo-thermo-mechanical variables associated with the half-space.

7 Numerical results and discussions

The objective of this section is to showcase the latest developments in the study of cutting-edge semiconductor materials, structures, and devices, alongside advancements in characterization methods that leverage plasma, thermal, elastic, and acoustic influences. These include techniques like carrierography, thermography, photothermal deflection, photothermal radiometry, etc. Additionally, a case study will be presented to highlight the numerical outcomes presented in previous sections. The effect of modifying parameters on mathematical solutions for physical quantities will also be explored. To facilitate the numerical computations, the characteristics of silicon (Si) will serve as a representative for semiconductor polymer materials. By considering $T_0 = 298\mathrm{K}$, the physical values for the introduced parameters are as follows [7]:

$$\begin{gathered} \{\lambda_e,\, \mu_e\} = \{2.696,\, 1.639\} \times 10^{10}\ \frac{\mathrm{kg}}{\mathrm{ms}^2},\quad \rho = 1740 \frac{\mathrm{kg}}{\mathrm{m}^3},\ \omega = 2\,\mathrm{rads}^{-1}, \\ K = 2.510\,\frac{\mathrm{W}}{\mathrm{m}}\mathrm{K},\quad C_E = 1.04 \times 10^3 \frac{\mathrm{Jkg}}{\mathrm{K}},\quad d_n = -\tfrac{9}{10^{31}}\ \mathrm{m}^3, \\ E_{\mathrm{g}} = 1.5077\,\mathrm{eV},\quad D_E = \tfrac{2.5}{10^3} \times \tfrac{\mathrm{m}^2}{s},\ s_{\mathrm{f}} = 2\frac{\mathrm{m}}{\mathrm{s}},\quad \tau = 5 \times 10^{-5}\ \mathrm{s}. \end{gathered}$$

The values of magnetic constants are considered as:

$$H_0 = \frac{10^7}{4\pi}\frac{\mathrm{A}}{\mathrm{m}},\ \varepsilon_0 = \frac{1}{36\pi \times 10^9}\frac{\mathrm{F}}{\mathrm{m}},\ \mu_0 = \frac{4\pi}{10^7}\frac{\mathrm{H}}{\mathrm{m}}.$$

Moreover, the following values are taken into consideration [40]:

$$R_G = 0.45\ \mathrm{mm},\ v = 10\ \mathrm{ns},\ \ \hat{R} = 91\%,\ \ \hat{\gamma} = 0.001\ \mathrm{m}^{-1},\ \hat{E} = 10\mathrm{J}$$

At $t = 0.12$ s, mathematical computations will be conducted through the use of Mathematica software. The characteristics and arrangements of all non-dimensional photothermal domains within semiconducting materials like silicon can be delineated by the aforementioned physical parameters. Furthermore, depictions of different domain variables' real-part plots will be exhibited within the median at surface $z = 0.2$. To explore the behavior of heated material, the patterns of thermal stress ($Re(\sigma_{zz}) = \widehat{\sigma}_{zz}$ and $Re(\sigma_{xz}) = \widehat{\sigma}_{xz}$), within a very short time, the variation of temperature $Re(\theta) = \widehat{\theta}$, the carrier density $Re(N) = \widehat{N}$, vertical displacement $Re(u) = \widehat{u}$, and changes in transverse (transverse) displacement $Re(w) = \widehat{w}$ are illustrated as a function of material's depth.

7.1 Effect of varying the rise time of the laser pulse

Knowing the location and magnitude of tension line-focused laser irradiation can prove to be valuable in certain situations. Examining the correlation between the field generated by the laser and surface-breaking fissures could be an intriguing avenue for exploration. The concept of the "scattered field," which comprises tractions on the surfaces of cracks, adds to the tractions induced by the "incident field" on the same surfaces, and ensures that the criterion for "traction-free crack surfaces" is satisfied, proving to be a useful tool in this case.

The duration of picosecond laser pulses' rise time is directly linked to the energy held within the pulse and the spot diameter. Moreover, it is confined to the silicon surface, which holds the greatest concentration of laser energy. In the subsequent subsection, we will delve into the thermal stress fields and deformations generated in a silicon half-space by line-focused laser light. Theoretical conclusions were drawn using the thermoelastic concept, which explores the movement of heat. The ongoing research analyzes laser-induced ultrasound with the aid of the generalized thermodynamic theory of elasticity.

Figures 1, 2, 3, 4, 5 and 6 demonstrate the impact of altering the laser pulse rise-time coefficient v ($v =$ 1.0, 1.1, and 1.2) on the system fields as a function of position x. The figures depict that all of the system fields satisfy the boundary conditions, with all curves converging as x approaches infinity. Notably, we observe that the rise-time factor v of the laser pulse has a significant effect on the studied fields for x values ranging from 0 to 10. In laser ultrasound, the correlation between heat and wave equations is driven by the concept of thermal expansion, resulting in a partially associated problem. In contrast, the extended thermoelasticity model accounts for temperature interaction of stress pulses as they propagate through the material, rendering the problem fully coupled. As a result, both thermal and elastic waves can be observed.

Figure 2 showcases how alterations in the laser pulse's rise-time coefficient v affect the temperature field $\widehat{\theta}$ at various distances x. As depicted, the temperature gradient initially reaches its maximum positive value at the boundary where the laser pulse is applied and gradually decreases to zero. The smallest temperature value is observed at $x = 7$. Furthermore, it has been observed that changes in the laser pulse rise-time v have a significant impact on the temperature fluctuation $\widehat{\theta}$, as the rise-time factor is directly proportional to both the time of the laser pulse and the temperature range. Thus, an increase in the laser pulse rise-time v results in a wider temperature range $\widehat{\theta}$, as demonstrated by the figure. It is worth noting that precise measurement of the temperature field is crucial for accurate prediction of laser-induced ultrasound since the temperature acts as the driving force of the ultrasound. The current computational model effectively simulates the rapid energy deposition of a single laser pulse in a transient thermoelastic volume.

Figure 3 illustrates the changes in the real part of the carrier density $\widehat{N}$ as a function of distance x and the laser pulse rise-time coefficient v. As shown, $\widehat{N}$ starts with positive values in all scenarios and steadily increases until it reaches its maximum potential before decreasing to zero. Based on recombination process calculations,

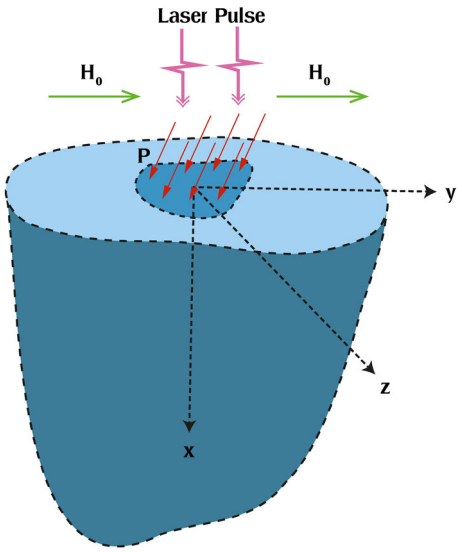

Fig. 1 Schematic configuration of a photothermal solid half-space

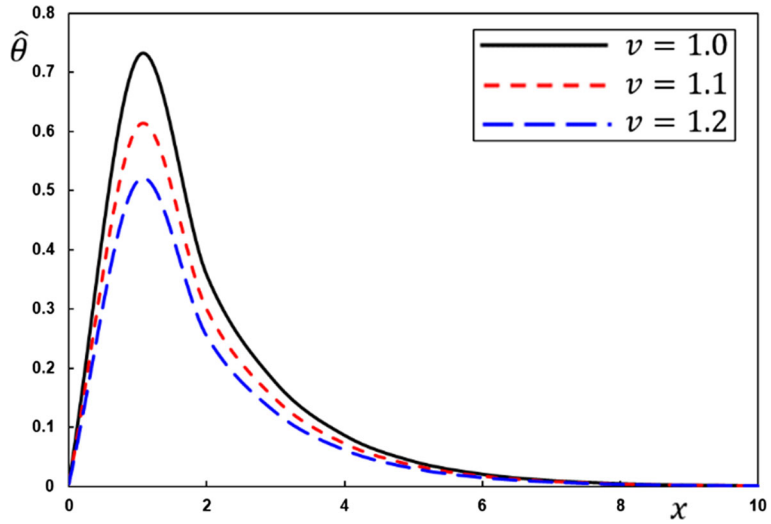

Fig. 2 The influence of rise-time coefficient v on temperature $\widehat{\theta}$

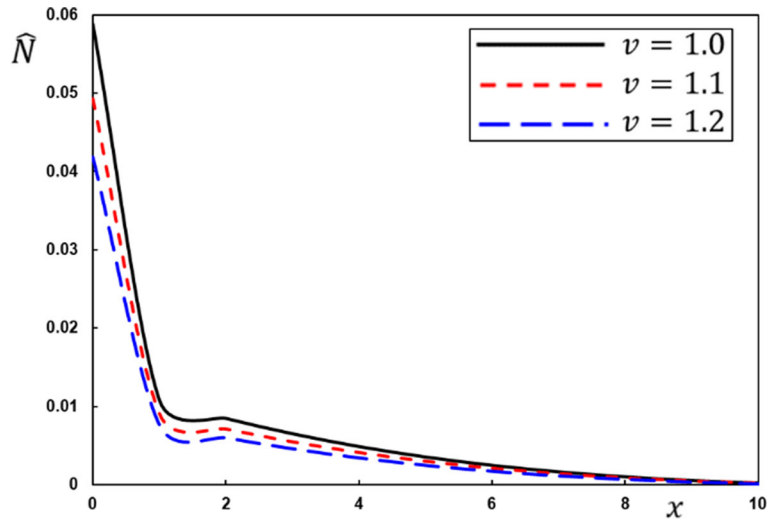

Fig. 3 The influence of rise-time coefficient v on carrier charge density $\widehat{N}$

plasma wave propagation begins with positive values that are expected to exist at the surface in all three v scenarios. The photo-excitation transfer operation then drives the plasma waves to become stronger, with the waves reaching their peak intensity near the surface. Notably, Fig. 3 clearly demonstrates the significant impact of the laser pulse rise-time coefficient v on the variations in carrier density $\widehat{N}$. The observed patterns serve as evidence of this effect. Specifically, when applying the improved 4MGT-PTVE photo-thermo-viscoelastic model, a decrease in the variation of $\widehat{N}$ was observed as the pulse rise-time factor v increased. This finding held true across all tested scenarios.

In Fig. 4, one can observe that the displacement $\widehat{u}$ exhibits a significant surface response, which gradually diminishes as depth x within the medium and time t increase. The behavior of the horizontal displacement component $\widehat{u}$ appears to be affected by the duration of the rising edge of the laser pulse v, as deduced from the illustrated results. Moving onto Fig. 5, we notice that the displacement $\widehat{w}$ varies with both depth x and time. Notably, the magnitude of the displacement $\widehat{w}$ is lower for values of v equal to 1.1 and 1.2 compared to 1.0. This phenomenon can be attributed to the prominent influence of the laser pulse time factor on the deformation.

As the distance from the laser line-axis source increases, the waveforms exhibit a wide range of shapes and amplitudes. The most prominent alterations in displacement can be observed on the irradiated surface. At the same time, the waveform is predominantly influenced by thermal events taking place directly under the source within the heated zone. Several studies [49–51] have investigated the vertical surface displacements obtained

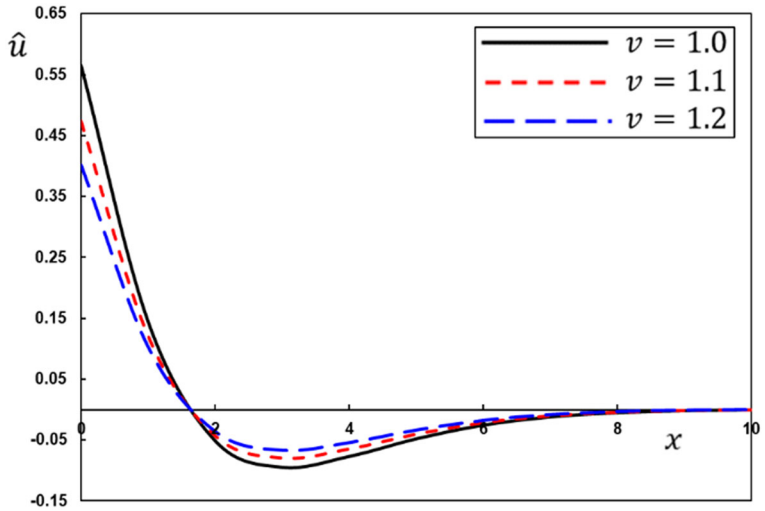

Fig. 4 The influence of rise-time coefficient v on displacement $\widehat{u}$

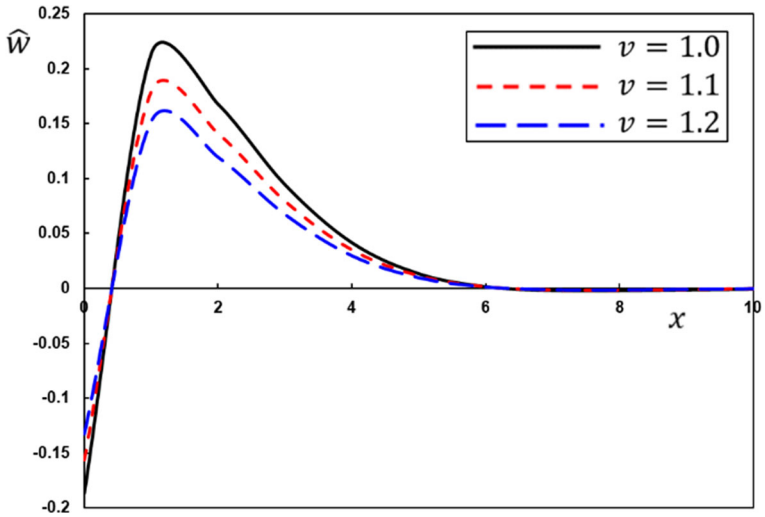

Fig. 5 The influence of rise-time coefficient v on displacement $\widehat{w}$

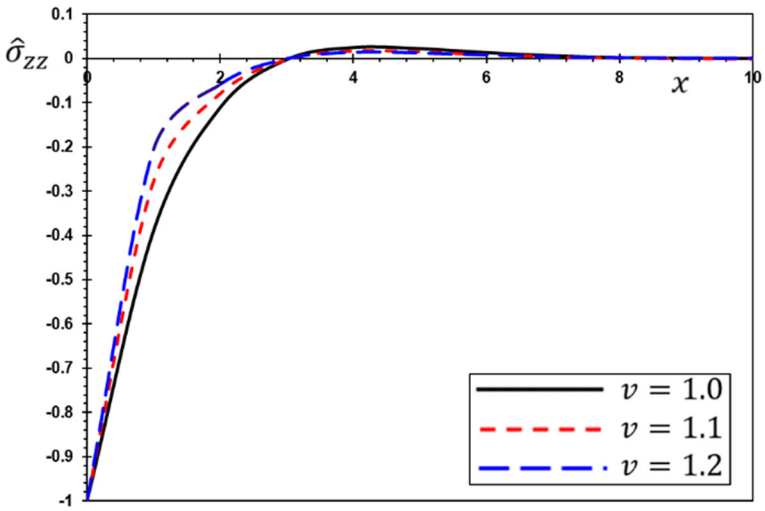

Fig. 6 The influence of rise-time coefficient v on stress $\widehat{\sigma}_{zz}$

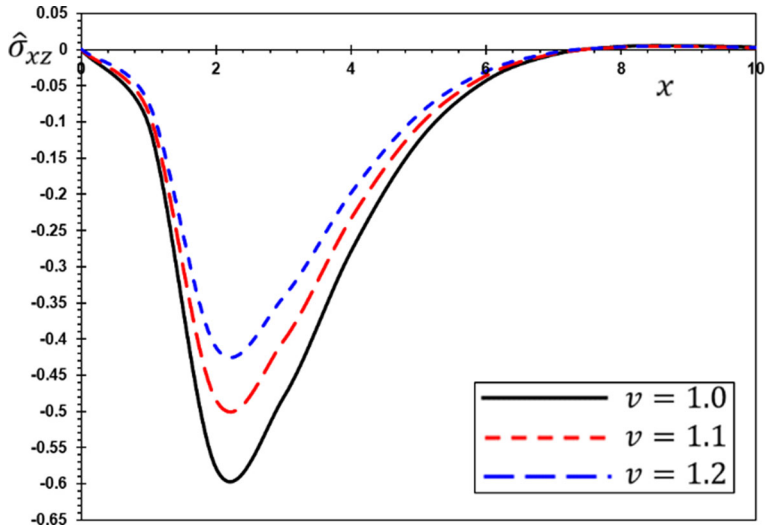

Fig. 7 Influence of rise-time coefficient v on stress $\widehat{\sigma}_{xz}$

experimentally from a point laser source within the heated zone. Remarkably, the results generally align with the predicted pattern suggested by theoretical models in the literature.

Figures 6 and 7 illustrate the differences in thermal stress characteristics $\widehat{\sigma}_{zz}$ and $\widehat{\sigma}_{xz}$ based on the distance x. The sensitivity for each of the three possible pulse rise-time factor v choices is almost identical, indicating their comparable effectiveness. The figures demonstrate a noticeable increase in the transient thermal stresses, $\widehat{\sigma}_{zz}$ and $\widehat{\sigma}_{xz}$, as the laser pulse's rise time increases. Additionally, it is worth noting that the curves for thermal stress $\widehat{\sigma}_{xz}$ always originate from zero, which satisfies the mechanical boundary conditions and validates the numerical results' accuracy. In all three cases, the stress $\widehat{\sigma}_{zz}$ initially rises dramatically before stabilizing, owing to the initial thermal stress applied along the z-axis. Furthermore, increasing the laser pulse's rise-time factor v leads to a significant shift in the magnitude and behavior of thermal stresses, as depicted in the figures.

For certain applications, it can be beneficial to have knowledge of the stress that is generated by irradiation using a laser that is concentrated along a particular line. Prior to calculating the dispersed field, one must first ascertain the stresses caused by the incident field. This necessitates measuring the stress field accurately in all directions, from a distance to close proximity to the source. When utilizing the scanning laser source method, whereby the laser source is moved across the test material, these measurements are particularly important. These findings are in line with those documented in relevant research literature, specifically sources [38, 39]. Although the results presented pertain to semiconductors, they suggest that the thickness of the semiconductor relative to the size of the irradiated region will play a crucial role in determining whether this simplified model may be used to forecast shifts at the epicenter during the generation of a laser within a semiconductor. The photo-thermoelastic model represents an excellent tool to obtain a highly precise estimate of the displacement of semiconductors at their edges.

The process of generating free electrons entails the swift movement of valence band electrons into the conduction band, resulting in the absorption of photons, as established by previous research [52]. This phenomenon is achieved using a nanosecond laser with an extremely high-power density. By utilizing a more powerful laser with a shorter pulse duration, we were able to increase the maximum number of liberated electrons [53]. It is worth noting that the depth to which the laser may penetrate the silicon is limited due to its high absorption rate. To achieve optimal results when treating silicone with a nanosecond laser, the pulse width should be kept to a minimum. This is due to the fact that a reduced pulse width leads to a higher lattice temperature at the surface. As such, this numerical study provides essential theoretical considerations for selecting the appropriate nanosecond laser.

7.2 The influence of mechanical relaxation times

The majority of materials exhibit some degree of viscoelastic behavior, whereby they may be deformed in various ways depending on their temperature. In the case of polymers, stress relaxation over time t may be

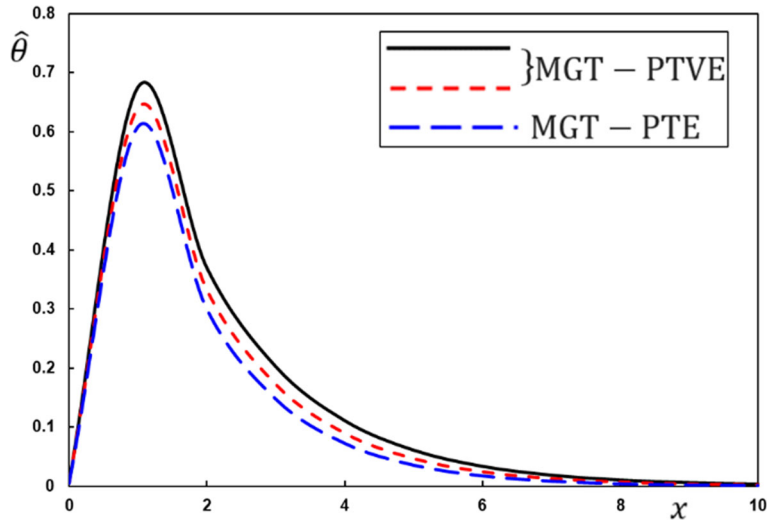

Fig. 8 The impact of viscosity on temperature $\widehat{\theta}$

described using their relaxation modulus (α_1 and α_2), which is a fundamental viscoelastic property of the material. To accurately analyze and design materials, it is crucial to realistically simulate tension relaxation and viscoelastic deformation across numerous subjects. The thermal transformations of viscoelastic materials may be characterized using free volume change or relaxation time. It is worth noting that while this research focuses primarily on the solid-state glass transition, it is important to acknowledge that the thermal transfer behaviors exhibited by different materials may vary depending on their specific properties.

Polymer scientists have introduced numerous physical hypotheses and models to describe the viscous behavior of materials, as well as their mechanical relaxation factors. In many of these simulations, linear viscosity was the principal focus, which is also the case in the present study. Among the most frequently utilized viscoelastic models for simulating a vibration isolator is the Voigt or Kelvin–Voigt model. The spring and damper elements in this model are arranged perpendicularly, with their properties combined to elucidate the elastic and viscous behaviors of the isolate. The modified Kelvin–Voigt method takes into account the viscoelastic behavior of polymers and illustrates how displacement over time corresponds to total strain.

Regarding the research and discussion presented in this work, both the general photothermal elasticity equations and the Kelvin model (MGT-PTVE) were taken into consideration. Specifically, we aim to investigate the effects of viscoelastic relaxation times, α_1 and α_2, by comparing scenarios with and without their presence ($\alpha_1 = 0.06$ and $\alpha_2 = 0.09$ vs. $\alpha_1 = \alpha_2 = 0$). Figures 8, 9, 10, 1111 and 12 provide numerical results comparing the viscosity effects of the two photothermal theory scenarios on the field variables studied (MGT-PTVE and MGT-PTE). When accounting for viscosity effects, we utilize the photo-thermo-viscoelasticity model (MGT-PTVE), whereas the photo-thermoelasticity model (MGT-PTE) is employed in its absence, assuming that all other settings remain constant. The response of photothermal visco-thermoelastic polymers to changes in displacement and temperature has not been previously examined.

Figure 8 depicts temperature distributions as a function of depth for two photothermal concepts, namely MGT-PTVE and MGT-PTE. The graph clearly illustrates that the MGT-PTE theory predicts significantly higher temperatures than the MGT-PTVE model. This suggests that incorporating viscoelastic relaxation durations α_1 and α_2 impedes the propagation of heat waves, in line with physical processes. It is worth noting that the rate of temperature diffusion is also constrained by the proposed model, consistent with the physical behavior of viscoelastic materials. The literature [54, 55] highlights the substantial temperature dependence of material properties which must be considered when investigating this type of material. Specifically, changes in temperature can alter the stiffness of a material, thereby influencing the amount of energy it dissipates during deformation.

Figure 9 demonstrates that the displacement $\widehat{w}$ exhibits a significant variation with changes in viscosity factors (α_1 and α_2) across a wide range of distances x. Specifically, we observe a decrease in displacement values as the viscosity is altered, with displacement curves declining at a faster rate. One may wonder why viscous or non-recoverable deformations appear to occupy a smaller volume than recoverable deformations. The answer lies in the fact that recoverable deformations undergo recovery, while non-recoverable deformations

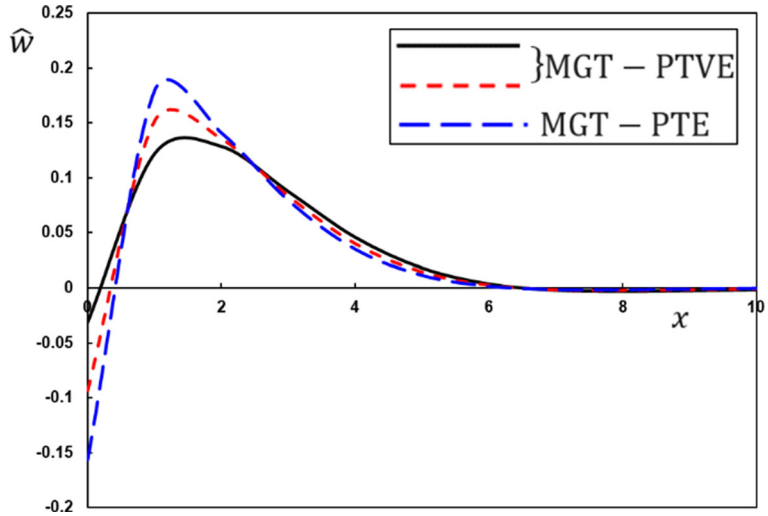

Fig. 9 The impact of viscosity on displacement $\widehat{w}$

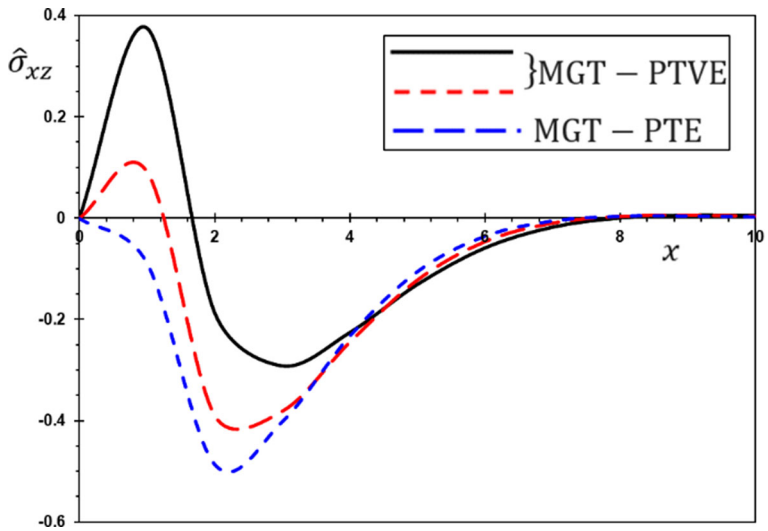

Fig. 10 The impact of viscosity on photothermal stress $\widehat{\sigma}_{xz}$

require much longer to complete than the same reversible deformation. This could be one explanation for this phenomenon.

Figure 10 showcases the correlation between photothermal stress $\widehat{\sigma}_{xz}$ and the distance x, with varying levels of the viscosity factor. The curves indicates that viscoelastic relaxation times play a significant role in affecting thermal stress $\widehat{\sigma}_{xz}$, while higher viscosity levels result in faster decreases in thermal stress. Moving onto Fig. 11, we observe fluctuations in carrier charge density $\widehat{N}$ versus x for the two photothermal hypotheses (MGT-PTVE and MGT-PTE). It is worth mentioning that the propagation speeds of these fields are limited, aligning with the brainwave patterns of viscoelastic materials, and suggesting that the amplitudes proposed by the photothermal visco-thermoelastic (MGT-PTVE) concept exceed those suggested by the photothermal thermoelastic (MGT-PTE) theory.

The findings of this case study hold implications across a wide range of scientific and technological fields, including atomic physics, industrial engineering, thermal energy plants, underwater constructions, compressed gases, aircraft design, chemical pipelines, and advanced materials. The current model demonstrates satisfactory emulation of both creep and harmonic behaviors under static and dynamic loadings. This model thus holds promising potential to replace the requirement for numerical and experimental simulations of viscoelastic processes in materials, leading to improvements in precision and simplicity. Notably, the simulated results

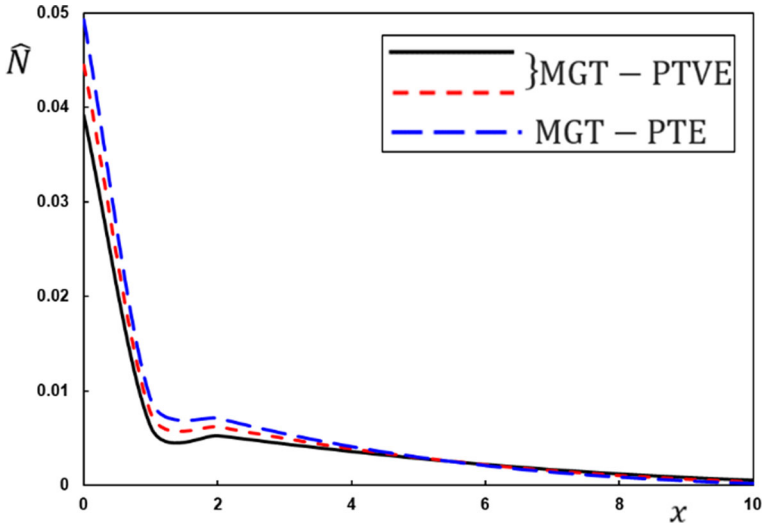

Fig. 11 The impact of viscosity on carrier charge density $\widehat{N}$

presented in this work were achieved through refined techniques as outlined in references [56, 57] and are highly accurate, thanks to careful experimental procedures.

8 Concluding remarks

This study focused on the photothermal interaction of a homogeneous, isotropic, semiconducting, and viscoelastic material within the framework of Moore–Gibson–Thompson (MGT) concepts of generalized photothermoelasticity. The Voigt and Kelvin model was incorporated to better understand viscoelastic materials and their viscosity, which depends on the speed at which they can relax and stress. To heat the semiconductor material, a laser pulse was utilized. Numerical simulations were conducted to explore how various physical parameters of the system affect the photophysical fields of a semiconductor in a thermo-viscous elastic medium.

Based on the findings of the present study, one can conclude the following results:

1. The semiconductor thermo-photophysical fields exhibit nonzero values only within a constrained area and consistently decrease without any thermal disruption outside this region. This outcome confirms that thermal and mechanical wavefronts in the model propagate at a limited rate with time.
2. The rise time of the laser pulse is a crucial component affecting the operation of all studied fields, as silicon's excellent energy absorption capability causes the beam's power to decrease as it penetrates deeper into the semiconductor material
3. Thermal stresses can result in surface and internal cracks in materials, complicating their ability to withstand high-temperature environments
4. Viscoelastic relaxation times slow down the transmission rate of thermomechanical waves, as per the proposed thermal conductivity equation. It is important to note that the speed of temperature diffusion is limited in viscoelastic materials, consistent with physical phenomena
5. By offering improvements in precision and simplicity, the proposed model has the potential to replace the need for numerical and experimental simulations of viscoelastic processes in materials
6. The study's results showcase the effectiveness of the proposed modeling and analysis methods for thermomechanical vibration in viscous Kelvin–Voigt semiconductor material
7. According to the findings of the research, thermodynamic and electronic deformation processes can significantly alter photothermal and acoustic signals, especially in proximity to the laser source impinging on the sample.

Acknowledgements H.M. Sedighi is grateful to the Research Council of Shahid Chamran University of Ahvaz for its financial support (Grant no. SCU.EM1401.98). The first three authors extend their appreciation to the Deputyship for Research & Innovation, Ministry of Education, Saudi Arabia, for funding this research work through the project number (IFKSURG-1232).

Author contributions All authors discussed the results, and the final text was reviewed through the contribution of all authors.

Declarations

Conflict of interest The authors declared no potential conflicts of interest with respect to the research, authorship and publication of this article.

References

1. Gafel, H.S.: Fractional order study of the impact of a photo thermal wave on a semiconducting medium under magnetic field and thermoplastic theories. Inf. Sci. Lett. **11**(2), 629–638 (2022)
2. McDonald, F.A., Wetsel, G.C., Jr.: Generalized theory of the photoacoustic effect. J. Appl. Phys. **49**(4), 2313–2322 (1978)
3. Stearns, R., Kino, G.: Effect of electronic strain on photoacoustic generation in silicon. Appl. Phys. Lett. **47**(10), 1048–1050 (1985)
4. Abbas, I.A., Alzahrani, F.S., Berto, F.: The effect of fractional derivative on photo-thermoelastic interaction in an infinite semiconducting medium with a cylindrical hole. Eng. Solid Mech. **6**, 275–284 (2018)
5. Todorović, D.: Photothermal and electronic elastic effects in microelectromechanical structures. Rev Sci Instrum **74**(1), 578–581 (2003)
6. Todorović, D.: Plasma, thermal, and elastic waves in semiconductors. Rev. Sci. Instrum. **74**(1), 582–585 (2003)
7. Song, Y.Q., Bai, J.T., Ren, Z.Y.: Study on the reflection of photothermal waves in a semiconducting medium under generalized thermoelastic theory. Acta Mech. **223**(7), 1545–1557 (2012)
8. Chteoui, R., Lotfy, Kh., El-Bary, A.A., Allan, M.M.: Hall current effect of magnetic-optical-elastic-thermal-diffusive non-local semiconductor model during electrons-holes excitation processes. Crystals **12**, 1680 (2022)
9. Sharma, N., Kumar, R.: Photo-thermoelastic investigation of semiconductor material due to distributed loads. J. Solid Mech. **13**(2), 202–212 (2021)
10. Alhejaili, W., Lotfy, Kh., El-Bary, A., Saeed, A.M., Roshdy, E.M.: Photo-thermo-mechanical-elastic interactions due to Hall current in functionally graded (FG) semiconductor excited medium with hyperbolic two-temperature. Alex. Eng. J. **61**(12), 11623–11633 (2022)
11. Mondal, S., Sur, A.: Photo-thermo-elastic wave propagation in an orthotropic semiconductor with a spherical cavity and memory responses. Waves Rand. Comp. Media **31**(6), 1835–1858 (2021)
12. Zakaria, K., Sirwah, M.A., Abouelregal, A.E., Rashid, A.: F, Photothermoelastic survey with memory-dependent response for a rotating solid cylinder under varying heat flux via dual phase lag model. Pramana. J. Phys. **96**, 219 (2022)
13. Abouelregal, A.E., Sedighi, H.M., Eremeyev, V.A.: Thermomagnetic behavior of a semiconductor material heated by pulsed excitation based on the fourth-order MGT photothermal model. Continuum Mech. Thermodyn. **35**(1), 81–102 (2022)
14. Abouelregal, A.E., Rayan, A., Mostafa, D.M.: Transient responses to an infinite solid with a spherical cavity according to the MGT thermo-diffusion model with fractional derivatives without nonsingular kernels. Waves Rand. Comp. Media (2022). https://doi.org/10.1080/17455030.2022.2147242
15. Feng, J., Safaei, B., Qin, Z., Chu, F.: Nature-inspired energy dissipation sandwich composites reinforced with high-friction graphene. Comp. Sci. Tech. **233**, 109925 (2023)
16. Safaei, B., Onyibo, E.C., Goren, M., Kotrasova, K., Yang, Z., Arman, S., Asmael, M.: Free vibration investigation on RVE of proposed honeycomb sandwich beam and material selection optimization. Facta Univ. Series Mech. Eng. **21**(1), 31–50 (2023)
17. Sarkon, G.K., Safaei, B., Kenevisi, M.S., Arman, S., Zeeshan, Q.: State-of-the-art review of machine learning applications in additive manufacturing; from design to manufacturing and property control. Arch. Computat. Methods Eng. **29**, 5663–5721 (2022)
18. İnada, A.A., Arman, S., Safaei, B.: A novel review on the efficiency of nanomaterials for solar energy storage systems. J. Energy Stor. **55**, 105661 (2022)
19. Alhijazi, M., Safaei, B., Zeeshan, Q., Arman, S., Asmael, M.: Prediction of elastic properties of thermoplastic composites with natural fibers. J. Text. Inst. (2022). https://doi.org/10.1080/00405000.2022.2131352
20. Lord, H.W., Shulman, Y.: A generalized dynamical theory of thermoelasticity. J. Mech. Phys. Solids **15**, 299–309 (1967)
21. Green, A.E., Lindsay, K.A.: Thermoelasticity. J. Elast. **2**, 1–7 (1972)
22. Tzou, D.Y.: A unified field approach for heat conduction from macro-to-microscale. J. Heat Transfer **117**, 8–16 (1995)
23. Tzou, D.Y.: Experimental support for the lagging behavior in heat propagation, Journal of Thermophys. Heat Transf. **9**(4), 686 (1995)
24. Green, A.E., Naghdi, P.M.: A re-examination of the basic postulates of thermomechanics. Proc. R. Soc. Lond. A. **432**, 171–194 (1991)
25. Green, A.E., Naghdi, P.M.: On undamped heat waves in an elastic solid. J. Therm. Stress. **15**(2), 253–264 (1992)
26. Green, A.E., Naghdi, P.M.: Thermoelasticity without energy dissipation. J. Elast. **31**(3), 189–208 (1993)
27. Roy Choudhuri, S.K.: On a thermoelastic three-phase-lag model. J. Therm. Stress **30**(3), 231–238 (2007)
28. Lasiecka, I., Wang, X.: Moore–Gibson–Thompson equation with memory, part II: general decay of energy. J. Diff. Equ. **259**(12), 7610–7635 (2015)
29. Quintanilla, R.: Moore–Gibson–Thompson thermoelasticity. Math. Mech. Solids **24**(12), 4020–4031 (2019)
30. Quintanilla, R.: Moore-Gibson-Thompson thermoelasticity with two temperatures. Appl. Eng. Sci. **1**, 100006 (2020)

31. Abouelregal, A.E.: Generalized thermoelastic MGT model for a functionally graded heterogeneous unbounded medium containing a spherical hole. Eur. Phys. J. Plus **137**, 953 (2022)
32. Abouelregal, A.E., Sedighi, H.M.: The effect of variable properties and rotation in a visco-thermoelastic orthotropic annular cylinder under the Moore–Gibson–Thompson heat conduction model. Proc. Inst. Mech. Eng. Part L J. Mat. Design Appl. **235**(5), 1004–1020 (2021)
33. Abouelregal, A.E., Alesemi, M.: Evaluation of the thermal and mechanical waves in anisotropic fiber-reinforced magnetic viscoelastic solid with temperature-dependent properties using the MGT thermoelastic model. Case Stud. Therm. Eng. **36**, 102187 (2022)
34. Abouelregal, A.E., Ersoy, H., Civalek, Ö.: Solution of Moore–Gibson–Thompson equation of an unbounded medium with a cylindrical hole. Mathematics **9**(13), 1536 (2021)
35. Sarkar, N., Mondal, S., Othman, M.I.A.: L-S theory for the propagation of the photothermal waves in a semiconducting nonlocal elastic medium. Waves Rand. Comp. Media **32**(6), 2622–2635 (2022)
36. Mallik, S.H., Kanoria, M.: Generalized thermoviscoelastic interaction due to periodically varying heat source with three-–phase–lag effect. Euro. J. Mech. A/Solids **29**, 695–703 (2010)
37. Sharma, S.R., Sharma, M.K., Sharma, D.K.: Vibrations of inhomogeneous visco thermoelastic nonlocal hollow sphere under the effect of three-phase-lag model. J. Solid Mech. **13**(1), 95–113 (2021)
38. Kong, J.A.: Theory of Electromagnetic Waves. John Wiley & Sons Inc, New York (1975)
39. Ball, D.W.: Field Guide to Spectroscopy. SPIE Press, Bellingham (2006)
40. Abouelregal, A.E., Mohammad-Sedighi, H., Shirazi, A.H., Malikan, M., Eremeyev, V.A.: Computational analysis of an infinite magneto-thermoelastic solid periodically dispersed with varying heat flow based on non-local Moore–Gibson–Thompson approach. Continuum Mech. Thermodyn. **34**(4), 1067–1085 (2022)
41. Nadeem, M., He, J.H., He, C.H., Sedighi, H.M., Shirazi, A.: A numerical solution of nonlinear fractional newell-whitehead-segel equation using natural transform. Twms J. Pure Appl. Math. **13**(2), 168–82 (2022)
42. Yavari, A., Abolbashari, M.H.: Generalized thermoelastic waves propagation in non-uniform rational b-spline rods under quadratic thermal shock loading using isogeometric approach. Iran J. Sci. Technol. Trans. Mech. Eng. **46**, 43–59 (2022)
43. Atta, D.: Thermal diffusion responses in an infinite medium with a spherical cavity using the atangana-baleanu fractional operator. J. Appl. Comput. Mech. **8**(4), 1358–1369 (2022)
44. Abouelregal, A.E., Mohammad-Sedighi, H., Faghidian, S.A., Shirazi, A.H.: Temperature-dependent physical characteristics of the rotating nonlocal nanobeams subject to a varying heat source and a dynamic load. Facta Univ. Ser. Mech. Eng. **19**(4), 633–656 (2021)
45. Jena, S.K., Chakraverty, S., Malikan, M., Mohammad-Sedighi, H.: Hygro-magnetic vibration of the single-walled carbon nanotube with nonlinear temperature distribution based on a modified beam theory and nonlocal strain gradient model. Int. J. Appl. Mech. **12**(05), 2050054 (2020)
46. Kaur, I., Singh, K.: Influence of time harmonic source frequency in a fibre-reinforced magneto-thermoelastic material with new modified couple stress and hyperbolic two-temperature theory. Iran J. Sci. Technol. Trans. Mech. Eng. (2022). https://doi.org/10.1007/s40997-022-00562-5
47. Awwad, E., Abouelregal, A.E., Hassan, A.: Thermoelastic memory-dependent responses to an infinite medium with a cylindrical hole and temperature-dependent properties. J. Appl. Comput. Mech. **7**(2), 870–882 (2021)
48. Arias, I., Achenbach, J.D.: Thermoelastic generation of ultrasound by line-focused laser irradiation. Int. J. Solids Struct. **40**(25), 6917–6935 (2003)
49. Askar, S., Abouelregal, A.E., Marin, M., Foul, A.: Photo-thermoelasticity heat transfer modeling with fractional differential actuators for stimulated nano-semiconductor media. Symmetry **15**, 656 (2023)
50. Spicer, J., Hurley, D.: Epicentral and near epicenter surface displacements on pulsed laser irradiated metallic surfaces. Appl. Phys. Lett. **68**(25), 3561–3563 (1996)
51. Veres, I.A., Berer, T., Burgholzer, P.: Numerical modeling of thermoelastic generation of ultrasound by laser irradiation in the coupled thermoelasticity. Ultrasonics **53**(1), 141–149 (2013)
52. McDonald, F.A.: On the precursor in laser-generated ultrasound waveforms in metals. Appl. Phys. Lett. **56**(3), 230–232 (1990)
53. Rämer, A., Osmani, O., Rethfeld, B.: Laser damage in silicon: energy absorption, relaxation, and transport. J. Appl. Phys. **116**(5), 053508 (2014)
54. Yang, J., Zhang, D., Wei, J., Shui, L., Pan, X., Lin, G., Sun, T., Tang, Y.: The effect of different pulse widths on lattice temperature variation of silicon under the action of a picosecond laser. Micromachines **13**, 1119 (2022)
55. Putignano, C., Reddyhoff, T., Dini, D.: The influence of temperature on viscoelastic friction properties. Tribol. Int. **100**, 338–343 (2016)
56. Carbone, G., Putignano, C.: A novel methodology to predict sliding/rolling friction in viscoelastic materials: theory and experiments. J. Mech. Phys. Solids **61**(8), 1822–1834 (2013)
57. Mei, M., He, Y., Wei, K., Duan, S., Li, M., Yang, X.: Modeling the temperature-dependent viscoelastic behavior of glass fabric with binder in the compaction process. Polym. Compos. **42**(6), 3038–3050 (2021)

Publisher's Note Springer Nature remains neutral with regard to jurisdictional claims in published maps and institutional affiliations.

Springer Nature or its licensor (e.g. a society or other partner) holds exclusive rights to this article under a publishing agreement with the author(s) or other rightsholder(s); author self-archiving of the accepted manuscript version of this article is solely governed by the terms of such publishing agreement and applicable law.